MODEL ANALYSIS OF REMOTELY CONTROLLED RENDEZVOUS AND DOCKING WITH DISPLAY PREDICTION

Paul Milgram and Paul H. Wewerinke
National Aerospace Laboratory NLR
Anthony Fokkerweg 2, 1059 CM Amsterdam, The Netherlands.

ABSTRACT

Manual control of rendezvous and docking (RVD) of two spacecraft in low earth orbit by a 'remote' human operator is discussed. Experimental evidence has shown that control performance degradation for large transmission delays (between spacecraft and operations control centre) can be substantially improved by the introduction of predictor displays. An initial Optimal Control Model (OCM) analysis of RVD translational and rotational perturbation control has been performed, with emphasis placed on the predictive capabilities of the combined Kalman estimator/optimal predictor with respect to control performance, for a range of time delays, motor noise levels and tracking axes. OCM predictions are then used as a reference for comparing tracking performance with a simple predictor display, as well as with no display prediction at all. Use is made here of an 'imperfect internal model' formulation, whereby it is assumed that the human operator has no knowledge of the system transmission delay.

1. INTRODUCTION

In the course of early missions in space (eg. Gemini, Apollo, Skylab), humans played an important role, especially during launch, early orbital phases and spacecraft systems checkout during actual flight. That role was often managerial; system variables were compared with nominal values and, in the case of unacceptable deviations, the spacecraft subsystem would be commanded to a standby or safety mode. In other space operations to date, including shuttle arm manoeuvres, furthermore, the human operator's (HO's) activities have been scheduled and well-defined and in practically all cases the HO's role has been very well rehearsed. For future space operations, especially contingency operations, on the other hand, faster responses and more adaptiveness, flexibility and innovation are going to be required.

During the execution of any (tele)operation in space, the HO, whether on the ground or in space, may be considered in some way to be 'remote' --i.e. spatially, temporally and/or functionally-- with respect to the system being supervised or controlled. The combination of remoteness and the need for extending human (perceptual, decision making and problem solving) capabilities into space will necessitate further technological developments both towards increasing local autonomy through artificial intelligence and towards

This work was carried out under contract no. 5594/83/NL/AN(SC) for the European Space Agency (ESA).

augmenting the HO's ability to influence events at a remote worksite through 'telepresence' (Akin et al, 1983). In order systematically to define and optimise the distribution of machine and human intelligence within such remote teleoperator systems, designers of these systems will need to base their decisions, among others, upon analytical quantitative predictions of the human operator's performance as a system supervisor and controller.

One of the most important operations in space is rendezvous and docking (RVD), whose purpose is to bring together and achieve a physical union between two orbiting spacecraft. The capability of achieving this physical union opens up the possibility of execution of a large variety of space operations, such as transfer of spacecraft or spacecraft elements to new orbits, removal of debris in space, assembly of spacecraft in orbit, maintenance of spacecraft and exchange of spacecraft payloads.

When RVD operations are performed with unmanned spacecraft, operations are controlled from a (ground-based) Operations Control Centre (OCC). Contact between the OCC and the space segment (both spacecraft) involves activities such as periodic checkout of spacecraft systems, calibration, transmission of go/no-go commands, monitoring of manoeuvres and, in a number of cases, on-line, closed loop control by a human operator at the OCC.

Direct communication between an OCC on the ground and the space segment is possible only when 'coverage' exists; that is, when there exists a data transmission path between ground segment and space segment, and vice versa. Direct coverage exists when the spacecraft are within the optical field of view of the OCC. However, the times at which this occurs may be inappropriate, and also very brief. Such difficulties can be overcome by using a Data Relay Satellite (DRS) in geostationary orbit. In all cases the transmitted signals will be delayed to some extent, for both uplink and downlink transmission, and these delays will in turn tend to diminish the ease and efficiency of regulating RVD from the OCC. Sources of signal time delays include data synchronisation and limited data transmission capacity (in both space segment and ground segment), distance to be travelled by the signal, data sampling and processing, data routing via one or more DRS's and a non-colocated ground antenna and OCC.

In this paper we present a model analysis of performance during manually controlled RVD for a hypothetical 'chaser'-'target' system, as illustrated in Fig. 1. The central aspect addressed here is the effect on performance of a communication time delay between the HO's control station and the RVD worksite and the improvement in performance which can be achieved through the introduction of display prediction. We have allowed the delay to range as an independent parameter of the analysis, between zero (representing RVD directed by the HO from within the chaser for example) and several seconds (representing RVD directed from the ground, with communication established via one or more DRS's and ground stations). The other factors which are examined here are the effects of multi-axis controlling and the effect of HO-injected disturbances. The direct manual control case has been chosen specifically in order to investigate the feasibility and limits of performance for this fundamental operational mode, since, in light of current progress in telepresence technology, manual control need not necessarily be regarded solely as a

mode of 'last resort'. Complete details of this analysis may be found in the reference by Milgram et al. (1984).

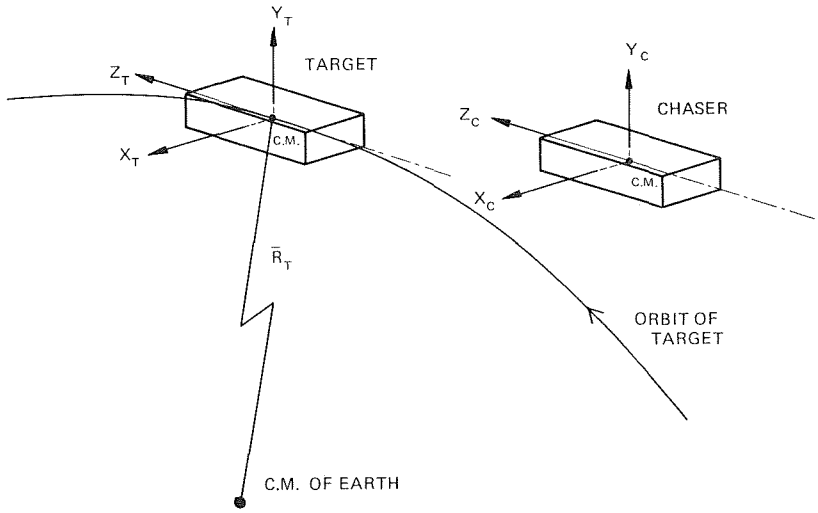

Fig. 1 Chaser-target reference frames.

2. OUTLINE OF ANALYSIS

A large number of early investigations into tracking performance in the presence of time delays have indicated that performance degrades rapidly as transmission delays increase, if continuous closed-loop tracking is attempted without some kind of mechanism for compensating for these delays. (Otherwise the HO will adopt an open-loop 'move-and-wait' control strategy.) Such mechanisms may be either extrinsic or intrinsic to the HO. Some common examples of extrinsic compensation devices include predictor displays, quickened displays, preview displays and 'flight director' displays. Even if no such external aids are supplied, the HO still possesses 'internal' information processing capabilities which act intrinsically to compensate for system delays, to an extent which depends upon the particular tracking situation (i.e. display characteristics, number of tracking axes, order and complexity of system dynamics, disturbance amplitude and bandwidth, etc.). This characteristic is modelled within the Optimal Estimator-Predictor part of the well known Optimal Control Model (OCM) (Kleinman, 1969; Kleinman et al, 1970).

In conventional applications of the OCM the HO is modelled specifically as being able, by means of the optimal predictor, to compensate for his/her own combined perceptual delays (along the order of 0.2 s). At what point the validity of such a delay compensation (sub)model breaks down for larger time delays, either intrinsic or extrinsic or combined, has not yet to our knowledge been carefully investigated. It will, as mentioned above, in any case depend on the characteristics of the task. In the analysis which follows, this aspect of the OCM has been extrapolated beyond its likely range of vali-

dity. In doing so we have not presumed that the HO is actually equipped with such inherent predictive capabilities. Rather, our first goal is to estimate an upper bound on performance, based on the usual assumed limitations of the human operator (observation noise, neuromotor noise) but excluding explicit perceptual delays (which have been neglected here relative to the much larger system transmission delays). By modelling a HO whose predictive capabilities are able to compensate optimally for extrinsic system transmission delays, what we obtain is an estimate of the best possible system performance, that is, the mean performance which might be expected when well-trained HO's are provided with an optimal predictor display.

Regarding such OCM results as forming a hypothetical upper bound on performance, given the constraints of the task and inherent limitations of the optimal predicting HO, it is convenient also to estimate a corresponding hypothetical lower bound on performance, based on exactly the same constraints, limitations and assumptions of optimality, but assuming that the HO performs no prediction. (The reason why this model is hypothetical is obvious: clearly the HO will always make some effort to compensate for system delay. The implication of not doing so is to presume that the HO zeroes system errors on the basis of currently displayed information, even though it is clear, on the basis of accumulated observations, that this is 'outdated' information.)

Finally, with respect to the above two cases, which collectively form a performance envelope for this analysis, we examine the case in which the HO is presented with a (simple) predictor display, which is designed to ameliorate tracking performance by performing the transmission time delay compensation extrinsically for the operator. By presenting the model results in this manner, i.e. in relation to the estimated performance envelope, it is clear i) what performance gains have been made by introducing the particular predictor display, and ii) what performance gains conceivably remain to be achieved with respect to optimal performance.

The optimal prediction modelling approach is outlined in the following section, and the no-prediction and predictor display analyses are described in section 4.

3. OPTIMAL PREDICTION MODEL

A schematic representation of the Optimal Control Model (OCM) as applied here is given in Fig. 2. In that figure both the uplink and downlink time delays, T_u and T_d, are indicated explicitly. In order to justify applying the OCM "as is" in the context of continuous tracking in the presence of communication time delays (and in the absence of extrinsic predictor aiding), we commence by postulating how such a "human optimal feedback controller" might conceivably behave under such circumstances. Assuming that, in addition to knowing the system dynamics and noise statistics, the HO also knows both the downlink and uplink delays, T_d and T_u, the essential elements of such a model are:

1. The HO receives noisy delayed display information, on the basis of which $\underline{\hat{x}}(t-T_d)$, an optimal estimate of the source of the T_d-delayed information from the remote system, is made.
2. The HO knows that if he/she were to generate a control command based upon an estimate of the present system state only, i.e. $\underline{\hat{x}}(t)$, such a command would arrive at the remote system at a time T_u too late. The HO must therefore generate a prediction of the future state of the remote system, i.e. $\underline{\hat{x}}(t+T_u)$, based upon past control inputs and past and present state estimates.
3. The HO generates a control signal, $\underline{u}_c(t)$, proportional to $\underline{\hat{x}}(t+T_u)$. The delayed input to the system in space, $\underline{u}_d(t)=\underline{u}_c(t-T_u)$, is the optimal control input.

On the basis of these hypotheses, and assuming stationarity, it can be shown that the 'conventional' approach to implementing the OCM can be used to analyse such optimal feedback regulation problems with up- and downlink delays simply by lumping together $T=T_u+T_d$ and substituting this delay into the standard OCM submodel of HO predictive compensation for internal perceptual time delays. In doing so we assume henceforth that the effects of the HO's own perceptual time delays are implicitly included within the total (lumped) system time delays.

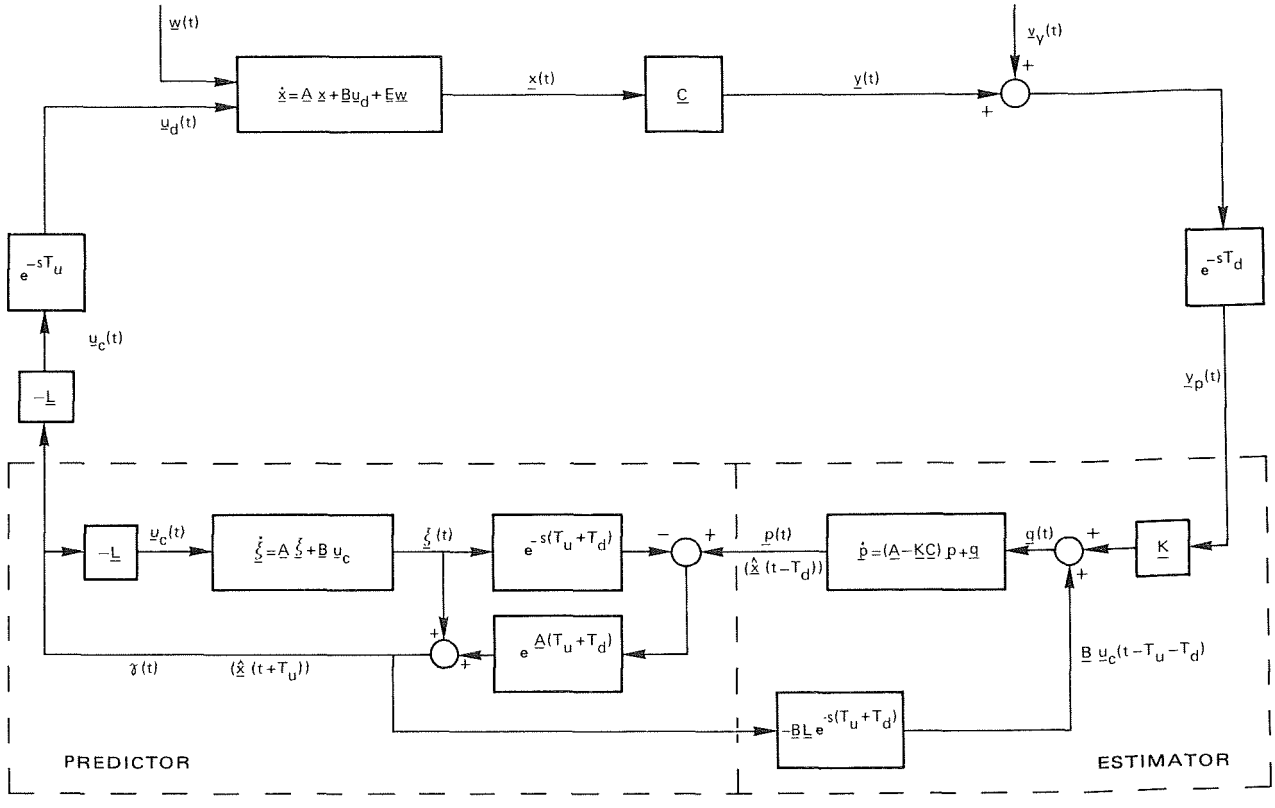

Fig. 2 Optimal feedback controller for system with up- and downlink time delay and observation noise.
(adapted from Kleinman, 1969)

4. NO-PREDICTION AND SIMPLE PREDICTOR DISPLAY MODELS

The essential difference between the above model and the model formulations used for the analysis of the no-prediction and the simple predictor display cases lies in the HO's knowledge of and response to the (lumped) system time delay. In the OCM analysis, where the optimal predictor is intrinsic to the HO, the HO is assumed to have perfect knowledge of the delay T. In the present two cases, however, prediction is either extrinsic (in the display) or completely absent. Since in these cases the HO is not required to have any knowledge of T, it is consequently assumed for the analysis that the HO has no knowledge of T. The reason for modelling these two cases in a similar fashion is that for both configurations the task of the operator is identical: to regulate out system disturbances on the basis of currently displayed information.

The absence of the HO's knowledge of T is a sufficient nonconformity from the conventional OCM structure to prevent us from employing the usual closed-form solution for ensemble average performance estimates. What is necessary is to formulate a model structure where the actual time delay is incorporated within the dynamic equations of the physical system, together with a model of the predictor display if there is one, but where the time delay is absent from the HO's internal model of that system. In other words, an analysis must be performed whereby the HO has an imperfect internal model of the physical system to be controlled.

As pointed out recently by Baron (1984), very little work has been done on modelling situations in which the system to be controlled is ill-defined for the HO. The approach taken here parallels that outlined in Baron & Berliner (1975) and the basic concepts are illustrated in Fig. 3. The formulation for the "real" system is expressed in the figure in the standard state space form as shown:

$$\dot{\underline{x}}(t) = \underline{A}\,\underline{x}(t) + \underline{B}\,\underline{u}_c(t) + \underline{E}\,\underline{w}(t) \qquad (1)$$

where $\underline{u}_c(t)$ is the HO's command input and $\underline{w}(t)$ is the independent, gaussian white system disturbance. Since the "real" system includes all physical elements external to the HO, if there is any transmission delay in the system it will be included in the upper block in Fig. 3. The display matrix ($\underline{C}$), including any predictive display, is also part of that block. The display information corrupted by observation noise which is perceived by the HO is expressed by:

$$\underline{y}_p(t) = \underline{C}\,\underline{x}(t) + \underline{v}_y(t) \qquad (2)$$

where $\underline{v}_y(t)$ is a gaussian, white noise. Note that for this analysis, as for the optimal prediction model above, we have neglected the human operator's own internal perceptual time delay.

Opposite the "real" system block in Fig. 3 is the HO's internal model of that system, which may or may not be the same, i.e. perfect. For the sake of generality the HO's internal model of the system is expressed in terms of a different state vector, $\underline{z}$, as shown:

$$\dot{\underline{z}} = \tilde{\underline{A}}\,\underline{z}(t) + \tilde{\underline{B}}\,\underline{u}_c(t) + \tilde{\underline{E}}\,\underline{w}(t) \qquad (3)$$

where the symbol $\tilde{}$ is used to distinguish the internal HO model parameters from those corresponding to the "real" system. The dimension of the HO's $\underline{z}$ vector may or may not be the same as $\underline{x}$. Whereas the HO's internal representation, as defined by the HO's $\tilde{\underline{A}}$, $\tilde{\underline{B}}$, $\tilde{\underline{C}}$, $\tilde{\underline{E}}$ matrices, may differ from the real system, the conventional assumption that the HO has a perfect internal representation of the covariance of the independent disturbance, $\underline{w}(t)$, of the observation noise $\underline{v}_y(t)$ and of his own injected motor noise, $\underline{v}_u(t)$, is retained for this analysis.

Similar to the OCM description above for no transmission delay, the HO is assumed to estimate the current presumed system state, $\hat{\underline{z}}(t)$, on the basis of both observed and expected display information, according to:

$$\dot{\hat{\underline{z}}}(t) = \tilde{\underline{A}}\,\hat{\underline{z}}(t) + \underline{B}\,\underline{u}_c(t) + \tilde{\underline{K}}\,(\underline{C}\,\underline{x}(t) + \underline{v}_y(t) - \tilde{\underline{C}}\,\hat{\underline{z}}(t)) \qquad (4)$$

where $\tilde{\underline{K}}$ is the HO's Kalman gain. Note that the bracketed expression on the right hand side of equation (4) is the difference between the current perceived information in equation (2) and the HO's expectation $\tilde{\underline{C}}\,\hat{\underline{z}}(t)$. Further-

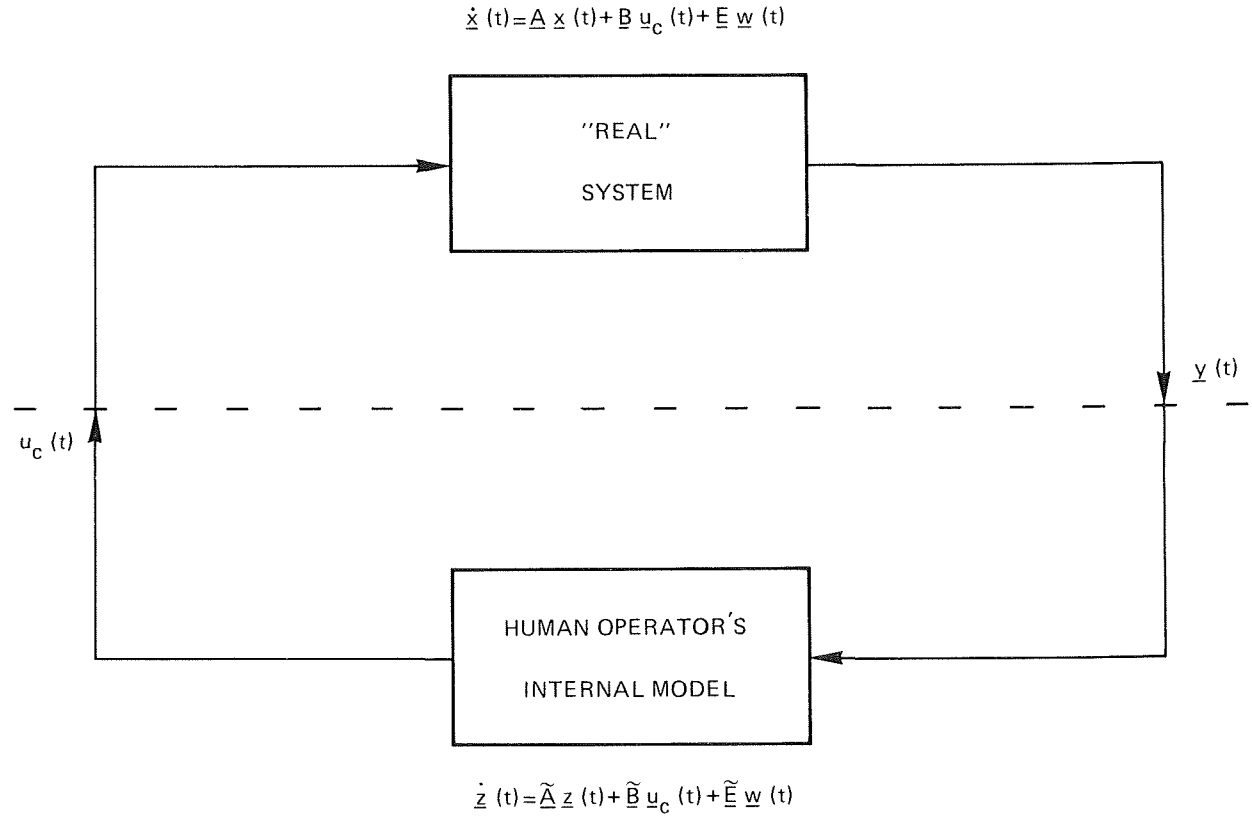

Fig. 3 Interface for imperfect internal model formulation.

more, as indicated also in Fig. 2, the HO is assumed to generate an optimal control command proportional to $\underline{\hat{z}}(t)$, given by:

$$\underline{u}_c(t) = -\underline{\tilde{L}}\,\underline{\hat{z}}(t) \tag{5}$$

which minimises a specified cost functional. The weighting factors which define this cost functional are assumed to be the same as for the optimal predictor case, since the goals of the task are the same for both cases. The $\underline{L}$ matrix must be computed on the basis of the $\underline{\tilde{A}}$ and $\underline{\tilde{B}}$ matrices, however, rather than on $\underline{A}$ and $\underline{B}$.

Substituting equation (5) into both equation (4) and equation (1), the results can be combined into a single linear system of matrix equations which describe the system in Fig. 3:

$$\begin{bmatrix} \dot{\underline{x}}(t) \\ \dot{\underline{\hat{z}}}(t) \end{bmatrix} = \begin{bmatrix} \underline{A} & -\underline{B}\,\underline{\tilde{L}} \\ \underline{\tilde{K}}\,\underline{C} & \underline{\tilde{A}} - \underline{\tilde{B}}\,\underline{\tilde{L}} - \underline{\tilde{K}}\,\underline{\tilde{C}} \end{bmatrix} \begin{bmatrix} \underline{x}(t) \\ \underline{\hat{z}}(t) \end{bmatrix} + \begin{bmatrix} \underline{E} & \underline{0} \\ \underline{0} & \underline{\tilde{K}} \end{bmatrix} \begin{bmatrix} \underline{w}(t) \\ \underline{v}_y(t) \end{bmatrix} \tag{6}$$

Assuming stationarity, the covariance of the combined $[\underline{x}\ \ \underline{\hat{z}}]'$ vector can be solved with conventional linear matrix operations.

The objective of incorporating the transmission time delay, T, within the actual system equations can easily be achieved by means of a linear Padé approximation. In the following analysis a second order Padé filter has been introduced at the output of the "real" system, that is:

$$\frac{o(s)}{i(s)} = \frac{1 - (1/2)Ts + (1/12)T^2s^2}{1 + (1/2)Ts + (1/12)T^2s^2} \tag{7}$$

which implies that, for an input i(t) to the filter, $o(t) \sim i(t-T)$. This results in $\underline{\tilde{A}}$ and $\underline{\tilde{B}}$ matrices which are sub-matrices of $\underline{A}$ and $\underline{B}$.

Since the HO part is modelled identically for the predictor display, no-prediction and OCM cases, the HO's $\underline{\tilde{C}}$ matrix is identical for each. In this analysis no explicit display format has been examined, i.e. display vectors = observable state vectors. For the no-prediction case the $\underline{C}$ matrix merely defines the delayed outputs as displays. To define the $\underline{C}$ matrix for the predictor case, a simple second order truncated Taylor series has been used for generating a displayed prediction of the system output component x(t):

$$y(t) = x(t) + T\,\dot{x}(t) + T^2/2\,\ddot{x}(t) \sim x(t+T) \tag{8}$$

Because third derivative information was unavailable, the observed rate of change of the predicted display is approximated by:

$$\dot{y}(t) = \dot{x}(t) + T\,\ddot{x}(t) \sim \dot{x}(t+T) \tag{9}$$

5. OUTLINE OF RVD FINAL APPROACH

The final approach phase of RVD is described in more detail in Milgram et al (1984). In summary, during station-keeping of the chaser at an aim point about 1000 m from the target, several activities are carried out on board both spacecraft, involving equipment checkout, readying of docking mechanisms, determination of relative position and attitude, etc. Upon receipt of a command from the OCC the chaser initiates the acquisition phase of RVD. The purpose of this phase is to bring the chaser from the aim point to a standoff point on the docking axis of the target, typically some 200 m from the target, upon which the chaser again engages in station-keeping and system checkout.

Upon receipt of another command from the OCC, the translation phase begins. The chaser now moves along the nominal docking axis of the target towards another standoff point some 20 m away from the target. Here further checks are carried out while the chaser is involved in station-keeping. The chaser then undergoes a series of controlled accelerations, decelerations and coasts, and finally achieves physical contact with the target, with carefully controlled relative translational and rotational errors and related rate errors.

In order to analyse this case it is clear that the various deceleration and acceleration manoeuvres from an initial to a final constant velocity constitute a terminal control problem. In the present RVD case, however, it has been specified that these manoeuvres are deterministically programmed for each flight profile. We therefore concentrate on the problem of regulating out disturbances, or perturbations, about the preprogrammed nominal flight profile and about the relative chaser-target orientation during constant velocity coasting. The problem of HO-mediated terminal controlling in RVD is nevertheless an important topic for future study.

The motion of each spacecraft (i.e. chaser and target) can be described in terms of translational motion of its centre of mass and rotational motion around its centre of mass. Roughly speaking, translation deals with position; rotation deals with orientation. In order to derive the equations of motion of relative position and relative orientation, certain assumptions have been introduced, specifically:

- the target moves in a near circular orbit around the Earth,
- the target is Earth-stabilised,
- the target docking axis lies along the principal axis of the target; in the nominal case this points in the direction of the orbital velocity vector (Fig. 1),
- the chaser reference frame is approximately aligned with the target reference frame; i.e. lateral position errors and their rates are small, orientation errors and their rates are small (Fig. 1),
- the chaser docking axis lies along the principal axis of the chaser.

These simplifications allow the relative translational perturbation dynamics to be expressed linearly as:

$$\ddot{x} = a_x - \omega_o^2 x$$

$$\ddot{y} = a_y + 3\omega_o^2 y + 2\omega_o \dot{z} \qquad (10)$$

$$\ddot{z} = a_z - 2\omega_o^2 \dot{y}$$

where ω_o is the orbital angular velocity and a_x, a_y, a_z are scaled thrust accelerations (in this case, maximum value = 0.01 m/s^2) along the respective axes. For positional control the goal is to reduce x,y (lateral errors) and z (deviation from programmed axial relative closure profile) and their derivatives to zero. For a circular low earth orbit of 500 Km, ω_o = 1.1 rad/s. Substituting this into equation (10) it can be demonstrated that all terms involving ω_o in the perturbation equations (10) are negligibly small, given the maximum thrust acceleration magnitudes of 0.01 m/s^2, whence it may be shown that the translational dynamics are effectively uncoupled. In the following, therefore, analyses are performed for one representative generic tracking axis from the uncoupled system of translational perturbation dynamics.

Turning to the rotational dynamics, it is assumed that the target is stabilised with respect to the orbital reference frame. The attitude motion of the chaser relative to the target is therefore given by:

$$\ddot{\theta} = m_x \,, \quad \ddot{\psi} = m_y \,, \quad \ddot{\phi} = m_z \qquad (11)$$

where θ, Ψ, ϕ are the angles of orientation of chaser with respect to target and m_x, m_y, m_z are scaled rotation control accelerations (in this case, maximum value = $1°/s^2$). Since the goal of attitude control is to zero the three uncoupled orientation angles, which have been assumed to be small, equations (11) may clearly be regarded as perturbation dynamics. Also for the analysis of rotational control, therefore, one representative generic tracking axis has been chosen.

In Table 1 the nominal limits on state deviations for the generic translational and rotational tracking axes are given. For translational control these limits are range (R) dependent, as shown. The values selected for this analysis have been indicated by an asterisk. These limits, which emphasise rate of change as opposed to positional deviation, define the control laws in the ensuing model analyses. (No other range dependent parameters have been assumed here. In particular, display outputs have been assumed equal to system state outputs. Had visual display cues been modelled explicitly, then range dependence would necessarily have to have been taken into account in this context.)

The specifying of the magnitude and statistical properties of external disturbances to this dynamic vehicular system is less straightforward, since most common 'terrestrial' factors, such as turbulence in the air or bumps on the road, are not present in space. The principle sources of noise which were assumed are:

i) fluctuations in the thruster outputs and thruster control system,
ii) cross-coupling between rotational and translational control systems,
iii) fluctuations in target attitude due to limit cycling in the attitude control system.

MAXIMUM POSITION MISALIGNMENT	* 0.5	(m)	(R ∿ 5 m)
	0.1	(m)	(R ∿ 1 m)
	0.02	(m)	(R ∿ 0.2 m)
MAXIMUM VELOCITY DEVIATION	* 0.01	(m/s)	(R ∿ 5 m)
	0.002	(m/s)	(R ∿ 1 m)
	0.0004	(m/s)	(R ∿ 0.2 m)
MAXIMUM ATTITUDE MISALIGNMENT	* 1.0	(deg)	
MAXIMUM ANGULAR VELOCITY DEVIATION	* 0.05	(deg/s)	

Table 1 Nominal limits on translational and rotational state deviations for generic chaser-target system.

Another, more unconventional, independent disturbance was assumed: (motor) noise introduced to the control system by the HO and which, due to the large time delays, propagates throughout the system and becomes effectively independent of the other state variables. In the following all independent system disturbances have been lumped and modelled collectively as a low-pass gaussian noise with bandwidth 0.2 rad/s and covariance equal to 1.5% of the related maximum thrust and maximum torque, for translation and rotation respectively. (The effect of varying bandwidth has also been analysed, but is not presented here.)

Another 'problem' associated with analysing such space propulsion systems is the bang-bang nature of control inputs, i.e. a thruster is either on or off. Such systems do not particularly lend themselves to straightforward linear, stationary analysis. However, if the thruster control logic is constructed such that command inputs are translated into trains of discrete firing pulses whose frequency determines the net effective thrust output (i.e. PFM, or pulse frequency modulation), it is possible to treat the HO's control input to the thrusters as quasi-linear and quasi-continuous. Such a PFM control logic was assumed in the following.

6. MODEL RESULTS

In Fig. 4 and 5 are shown the OCM results for translational and rotational motions respectively. In both figures the standard deviation of the positional component is shown on the left and of the velocity component on the right. The second independent parameter in both figures is the HO's motor noise-to-signal ratio, P_u, representing the relative amount of noise (in dB) injected by the HO into the system via his/her control actions. The reason for allowing P_u to vary in this fashion is due to uncertainty about precise levels of external disturbance, $\underline{w}(t)$, to the system. Since, as men-

tioned above, we are assuming that the HO is a potential source of approximately independent noise, the effect of different disturbance levels has been investigated in this fashion.

Since the noise levels examined here are relatively low, the performance for 'nominal' levels of P_u = -20 dB is quite stable in Fig 4 and 5; the HO/optimal predictor-controller is able to regulate the system quite well, even up to 10s delay. As relative noise level increases, however, performance becomes rapidly more divergent. This effect is more pronounced for rotational control, where noise levels do not go beyond P_u = -8 dB.

Relating these results to Table 1, we note that the 3σ levels in Fig. 4a and b remain well below the specified limits of 0.5 m and 0.01 m/s respectively over the ranges shown, for P_u = -20 dB and -10 dB. Comparing these to the rotational results in Fig. 5, however, we see that the 3σ levels exceed the specified maximum attitude misalignment and angular velocity deviation at approximately T = 1s and T = 0s respectively, for a (noisy) P_u of -10 dB. Clearly, the relative state and control weightings and comparative independent disturbance noise level for rotational control are such that this is a more difficult control task than translational control.

In both Fig. 4 and 5 the performance results are for one representative axis out of the three which are being simultaneously tracked. A 'full' attention level (P_o) of -17 dB has been assumed for each task (Baron, 1984). In Fig. 4 attention is evenly allocated across positional and velocity components; in Fig. 5, on the other hand, an optimal distribution of attention has been used. A separate analysis has confirmed, however, that due to low sensitivity in this region, the effective difference between the two approaches here is very slight.

In Fig. 6 and 7 are shown the results of varying the number of axes of tracking, i.e. 1, 3 or 6 axes. This has been simulated by means of varying the relative fraction of 'full' attention allocated across the various display outputs (eg. see Baron, 1984). The results are qualitatively similar for both translational and rotational performance. The important conclusion to be drawn from these results is that, although performance decrements in the direction expected as the human optimal estimator-controller is required to divide attention across increasingly more task dimensions, this performance decrement is not very large, that is, for the particular independent and dependent noise conditions which have been assumed. On the other hand, it can be expected that, as noise levels increase, the effect of multi-axis tracking will become more dramatic. This is because for higher noise levels the HO's uncertainty about the state of the system will become relatively greater more quickly. The consequence of this is that new displayed information becomes more important as expectations based on past observations become more unreliable. If under such circumstances the HO is required to allocate attention over more axes, the updating of display information will fall behind, total uncertainty will increase and performance will deteriorate.

OCM results from Fig. 4 and 5, for the intermediate case P_u = -14 dB, have been plotted in Fig. 9 and 10, together with the model results for the

no-prediction and predictor display analyses described above in section 4. In order to arrive at these results, a rather lengthy empirical attention optimisation procedure was followed, which is illustrated here in Fig. 8, for translational control. In that figure, where the selected optimal attention allocation is indicated by arrowheads, we see that, for increasing system time delay, velocity display information (equation 9) becomes less reliable and the HO must pay increasingly more attention to positional information (equation 8). Further details of the iterative algorithm necessary to generate the results in Fig. 9 and 10 for constant P_u are given in Milgram et al (1984).

Referring to Fig. 9 and 10, it must be noted that the abscissae differ in scale from those of Fig. 4 and 5. Note as well in Fig. 9 that for T = 1s numerical inaccuracy in the predictor and no-prediction estimates is indicated by a separate symbol.

As expected, Fig. 9 and 10 indicate best performance for the optimal predictor, worst performance for the no-prediction case and intermediate performance for the Taylor predictor display. It is perhaps surprising, in contrast to what might otherwise be suggested from previous experimental evidence, that the no-prediction performance has been maintained at all within the 3s range before diverging. The explanation for this can be shown to derive from the specific optimal control laws which have been computed and which have the equivalent effect of a large HO lead compensation. Evaluation of the validity of such control laws must explicitly take into account, however, the HO's visual thresholds for the observation of velocity information, which is necessary for realising the prescribed feedback control.

The principle factor underlying the control performance here, therefore, is the proportionately large weight assigned to minimising velocity deviations relative to positional misalignments, as indicated in Table 1. Indeed, we note that on the right hand sides of Fig. 9 and 10, i.e. for velocity deviations, the curves shown much more closely the expected pattern of rapid divergence of the no-prediction case as T increases and stabler performance for the Taylor predictor case. Clearly, a 'better' predictor display than the simple display defined in equations (8) and (9) would generate less rapidly increasing system output errors and would thus be able to extend the controllable time delay range even further, the limit of course being an 'optimal' predictor display, whose performance is indicated by the OCM curves.

7. CONCLUDING REMARKS

In this paper some factors related to the control of rendezvous and docking of two spacecraft in low earth orbit by a 'remote' human operator have been dealt with. In general, the remote control of systems in space, especially in the presence of large transmission delays, has long been recognised as a task which is ill-suited for the unaided human controller, and thus as a task which should be as fully automated as possible. As the need for more flexibility during scheduled and unscheduled operations grows, however, so will the need for more onsite 'intelligence'. One potential way to

bring the HO 'closer' to the remote sight is to compensate for transmission time delays by means of predictor displays (of all relevant sensory information). The model results presented in this paper provide an initial indication of some of the improvements in performance which may be gained through the use of such displays.

This paper has also attempted to illustrate the usefulness of adapting and applying existing human performance models for the analysis of this relatively unexplored class of human operator control problems. Further analyses are necessary in order to investigate the effects on performance, for example, of different external disturbance characteristics, different system dynamics and various advanced display concepts, including other predictor displays and integrated display formats such as perspective displays, preview displays and director displays. In addition to the application of existing models, new modelling approaches must be developed, including improved 'imperfect internal model' formulations, terminal control applications and open-loop 'move-and-wait' control models. The ultimate goal of these developments is to combine the use of skill-based behaviour models with models of cognitively more complex rule-based, and eventually knowledge-based, supervisory control behaviour, in order to be able systematically to analyse and evaluate a large range of potential teleoperator design alternatives and operational procedures.

8. REFERENCES

Akin, D.L., M.L. Minsky, E.D. Thiel and C.R. Kurtzman (1983): Space applications of automation, robotics and machine intelligence systems (ARAMIS), Phase II. NASA CR-3736.

Baron, S. (1984): Adaptive behaviour in manual control and the optimal control model; in Adaptive Control of Ill-defined Systems, O.G. Selfridge, E.L. Rissland & M.A. Arbib (ed's), Plenum Press, 51-73.

Baron, S. and J.E. Berliner (1975): MANMOD 1975: Human internal models and scene-perception model. U.S. Army Missile Command, TR RD-CR-76-3.

Kleinman, D.L. (1969): Optimal control of linear systems with time-delay and observation noise. IEEE Transactions on Automatic Control, Vol. AC-14, 524-526.

Milgram, P., P.Th.L.M. van Woerkom and P.H. Wewerinke (1984): Control loops with human operators in space operations; Part III: Rendezvous and docking operations and model analysis of performance with human-in-the-loop. (Netherlands) National Aerospace Laboratory, NLR Report TR 84116 L, Part III.

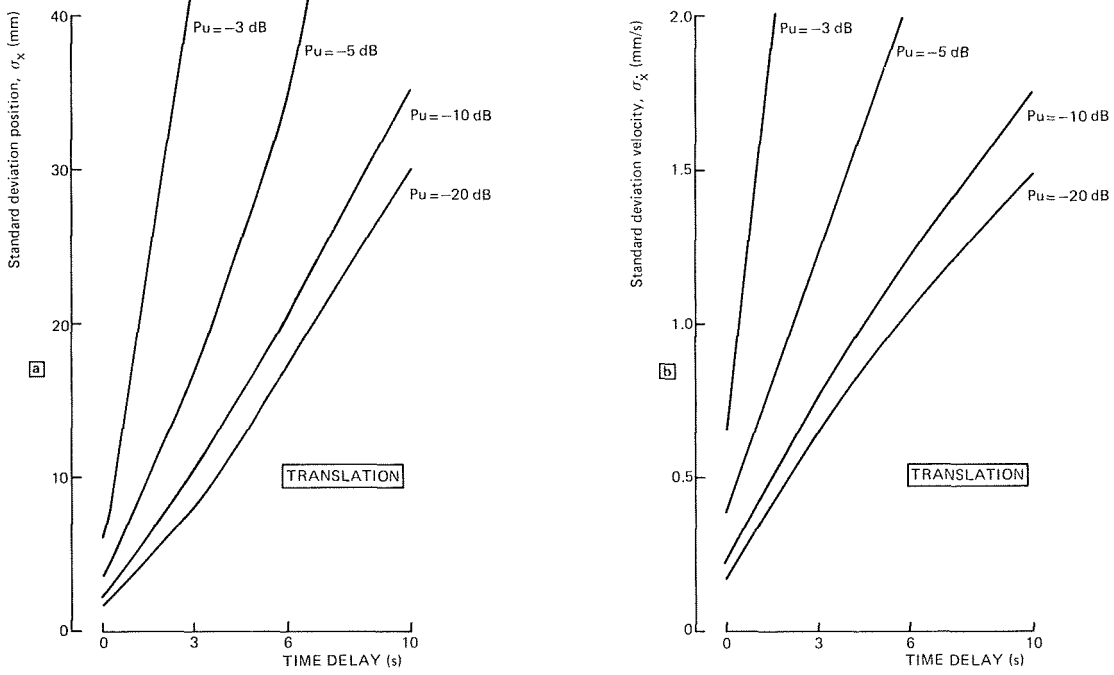

Fig. 4 Translational control: {(a) Position deviation / (b) Velocity deviation} vs time delay
For various motor noise levels (P_u)
(3-axis tracking: P_o = -17 dB, $f_1 = f_2 = 1/6$)

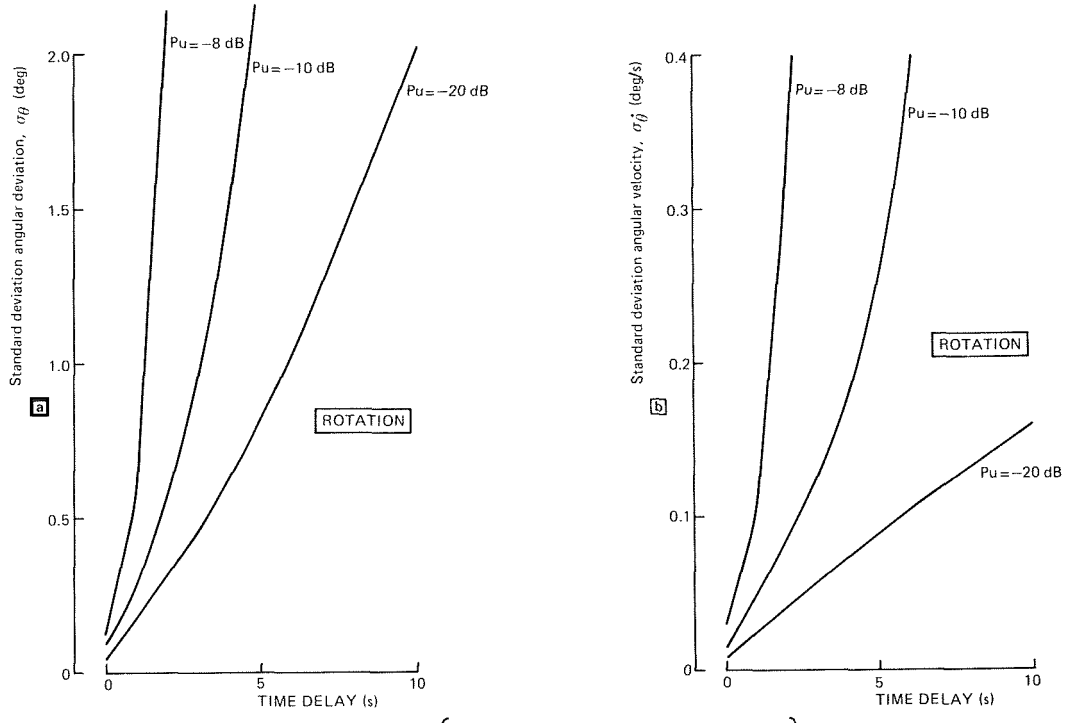

Fig. 5 Rotational control: {(a) Angular deviation / (b) Angular velocity} vs time delay
For various motor noise levels (3-axis tracking:
P_o = -17 dB, optimal attention)

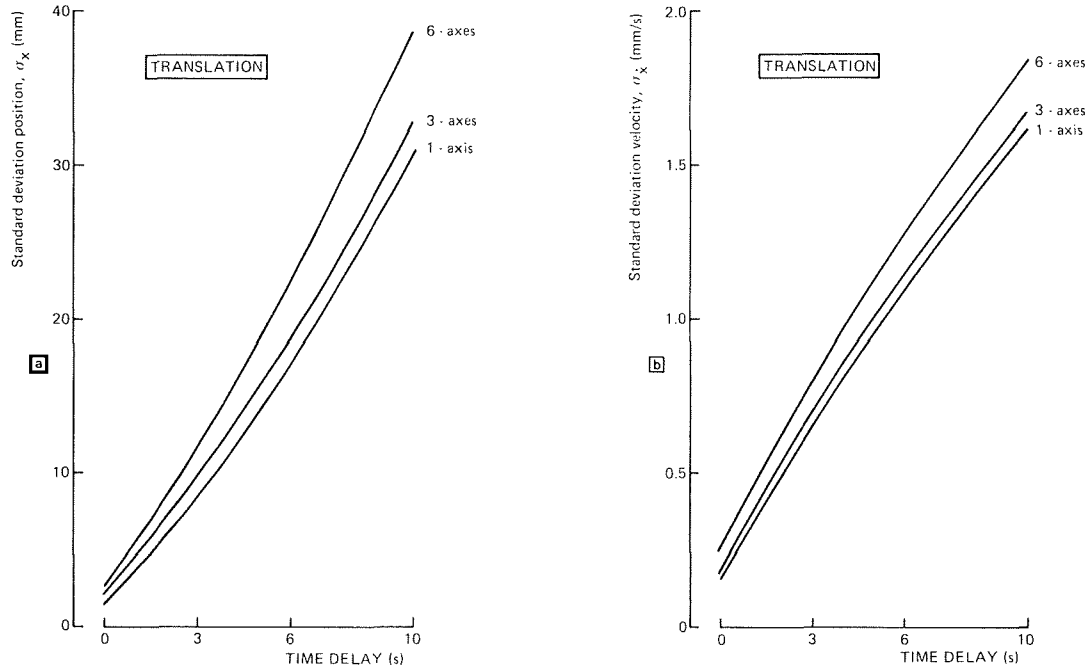

Fig. 6 Translational control: {(a) Position deviation / (b) Velocity deviation} vs time delay
For 1-, 3-, 6-axes of tracking.
(Optimal attention allocation, P_u = -10 dB)

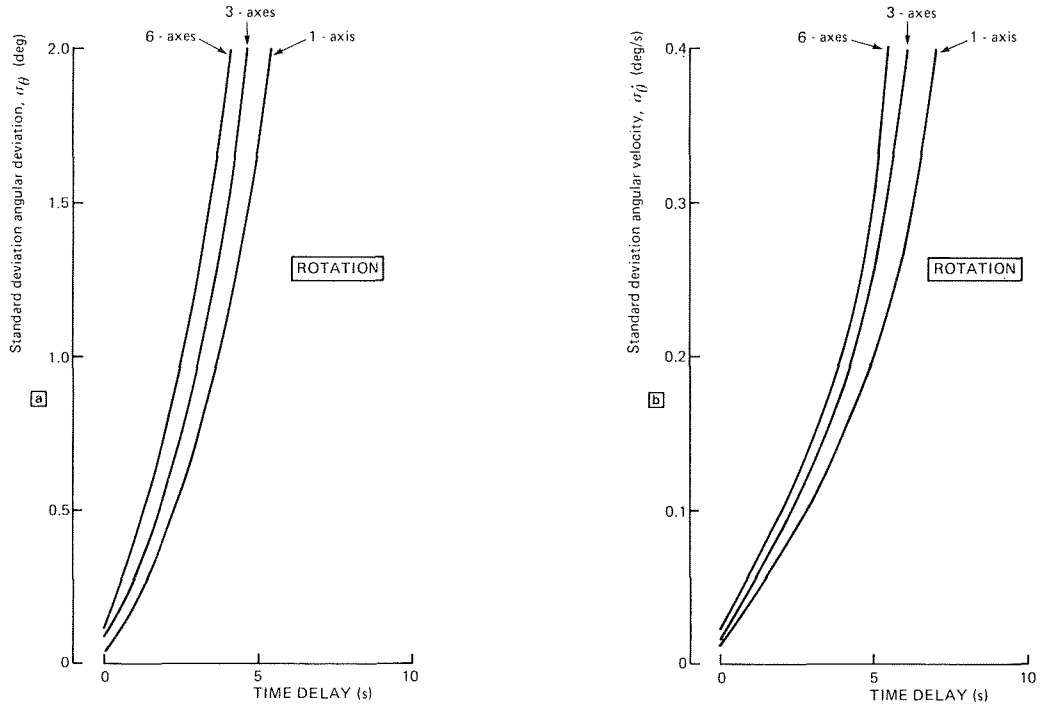

Fig. 7 Rotational control: {(a) Angular deviation / (b) Angular velocity} vs time delay
For 1-, 3-, 6-axes of tracking.
(Optimal attention allocation, P_u = -10 dB)

C - 5

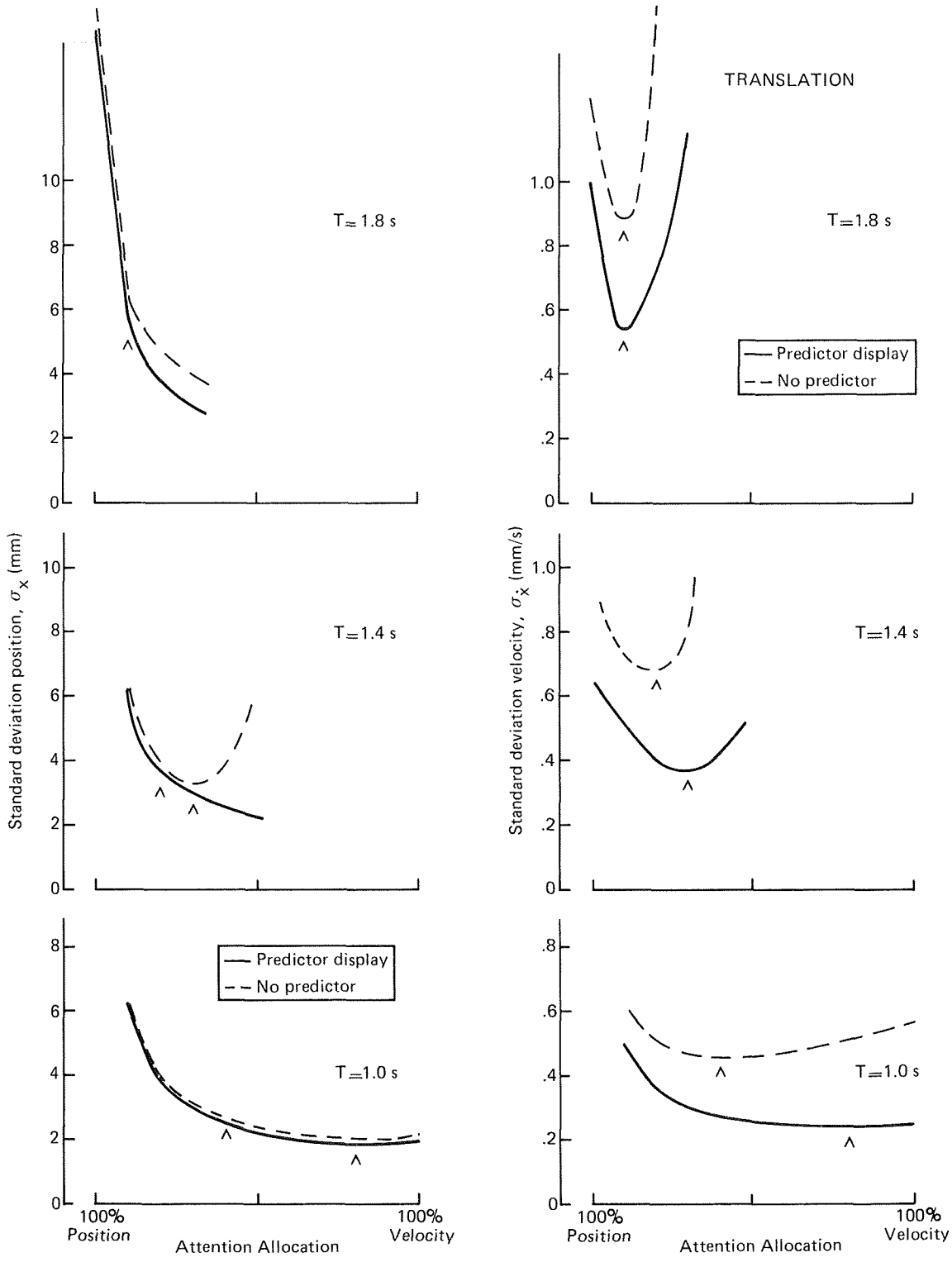

Fig. 8 Translational control: predictor and no-predictor display performance vs. attention allocation strategy for three time delays (3-axis tracking, p_o = -17 dB, $f_1 + f_2 = 1/3$)

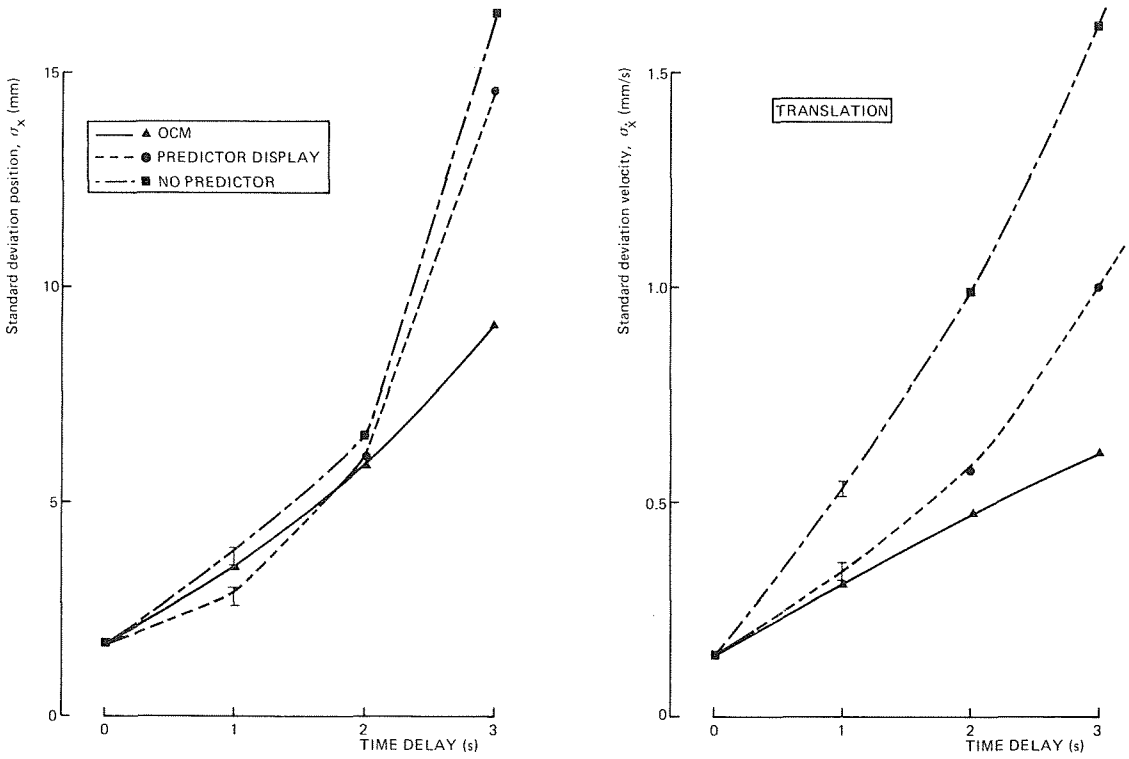

Fig. 9 Translational control: comparison of OCM, predictor display and no-predictor performance (3-axis tracking, optimal attention. P_o = -17 dB, P_u = -14 dB)

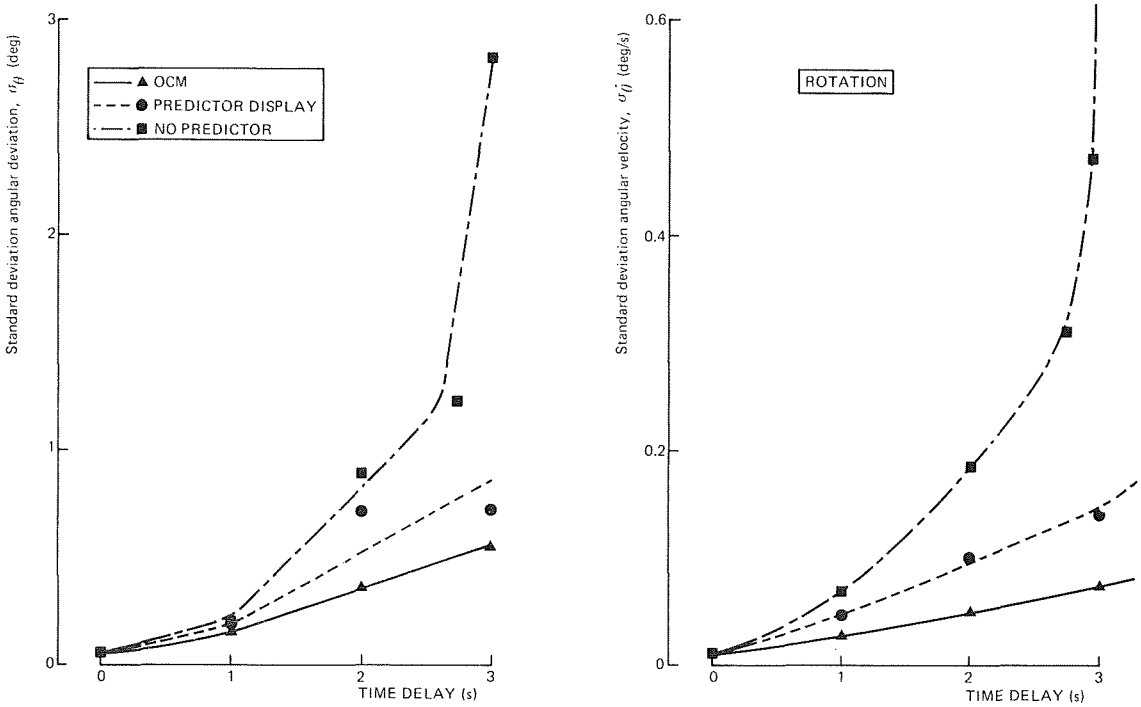

Fig. 10 Rotational control: comparison of OCM, predictor display and no-predictor performances (3-axis tracking, optimal attention, P_o = -17 dB, P_u = -14 dB)